Supporting information

Surface reconstruction on Ni_2P@CC to form an ultrathin layer of $Ni(OH)_2$ for enhancing capture and catalytic conversion of polysulfides in lithium-sulfur batteries

Lin Peng [a, b], Meixiu Qu [a, b], Rui Sun [a, b], Weiwei Yang [a, b], Zhenhua Wang [b], Wang Sun [b], Yu Bai [a, b, *]

[a] Advanced Research Institute of Multidisciplinary Science, Beijing Institute of Technology, Beijing 100081, PR China.

[b] Beijing Key Laboratory for Chemical Power Source and Green Catalysis, School of Chemistry and Chemical Engineering, Beijing Institute of Technology, Beijing,100081, PR China.

*Corresponding author: E-mail: yubaiit@163.com

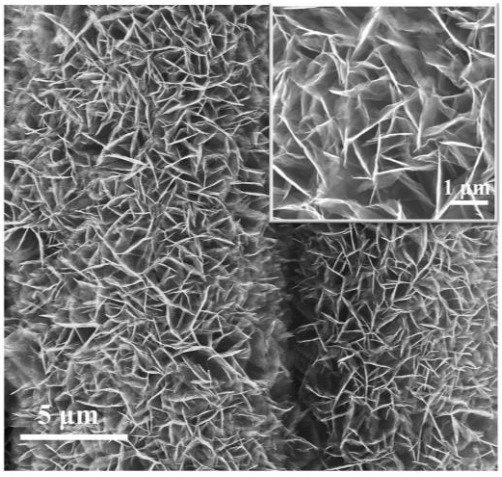

Fig. S1. SEM image of Ni_2P@CC (Insert is the magnified SEM image of Ni_2P@CC).

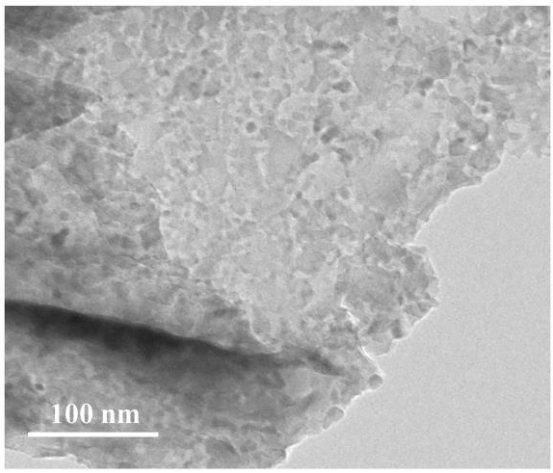

Fig. S2. TEM image of Ni_2P.

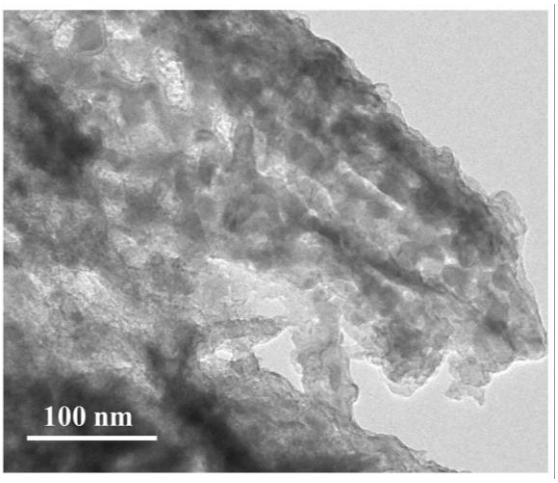

Fig. S3. TEM image of $Ni(OH)_2$-Ni_2P.

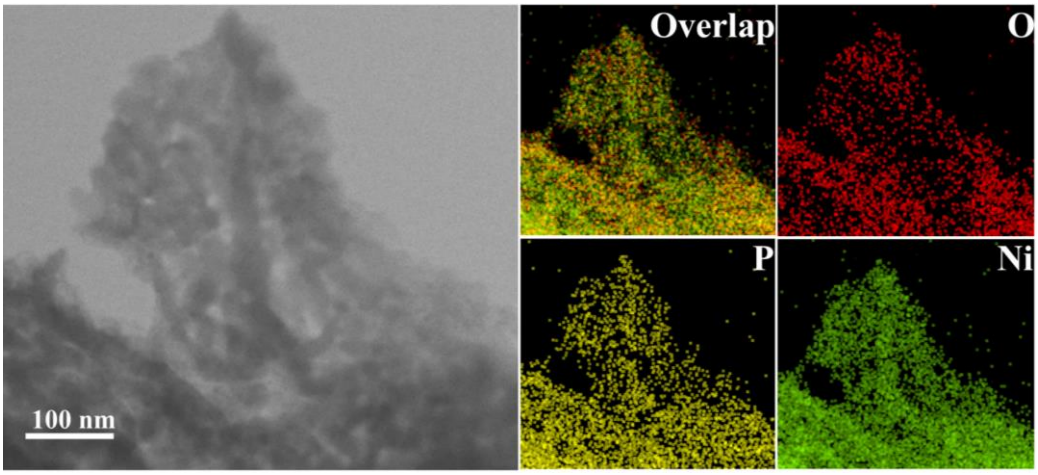

Fig. S4. HAADF-STEM image of $Ni(OH)_2$-Ni_2P@CC and the corresponding elemental mappings of overlap, O, P and Ni.

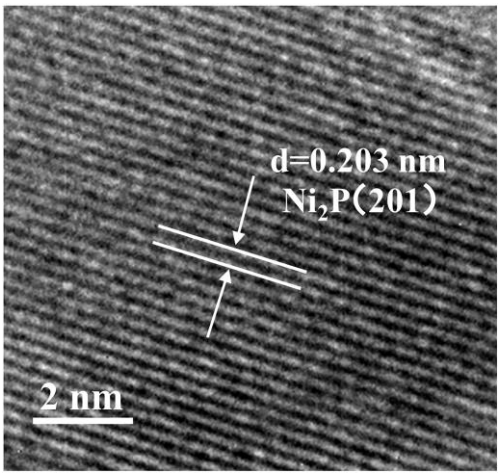

Fig. S5. HRTEM image of Ni_2P.

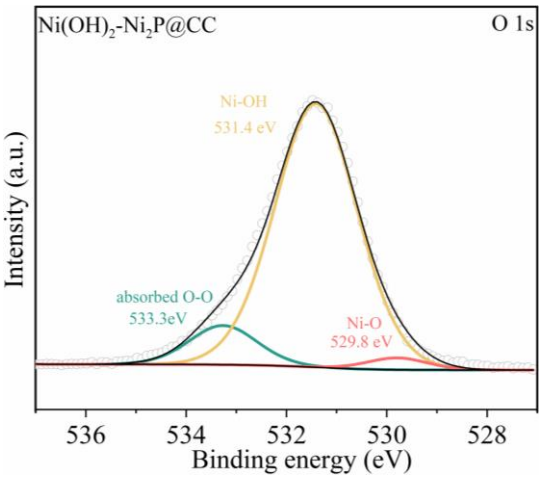

Fig. S6. The O 1s XPS spectrum of $Ni(OH)_2$-Ni_2P@CC.

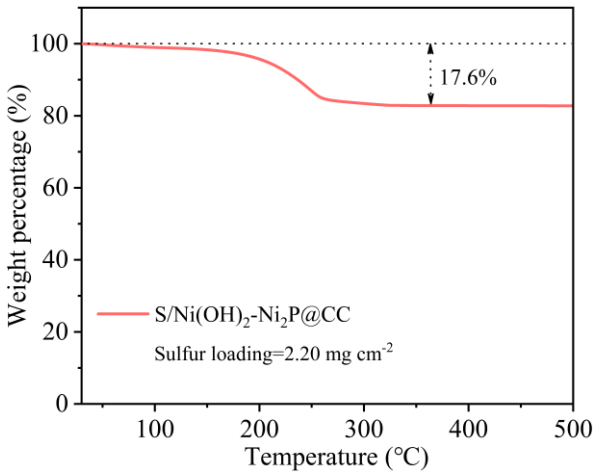

Fig. S7. TGA curve of S/Ni(OH)$_2$-Ni$_2$P@CC with a sulfur loading of 2.20mg cm^{-2}.

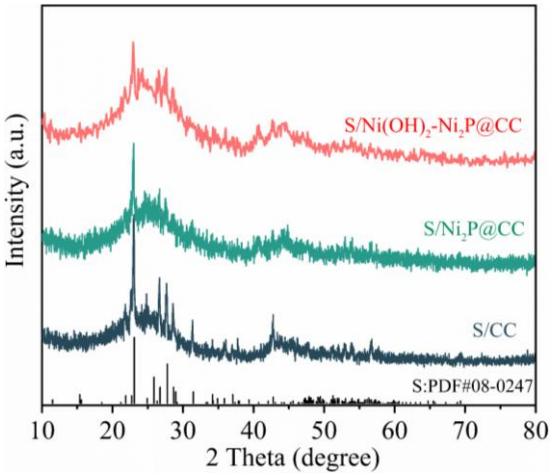

Fig. S8. XRD patterns of S/Ni(OH)$_2$-Ni$_2$P@CC, S/Ni$_2$P@CC and S/CC.

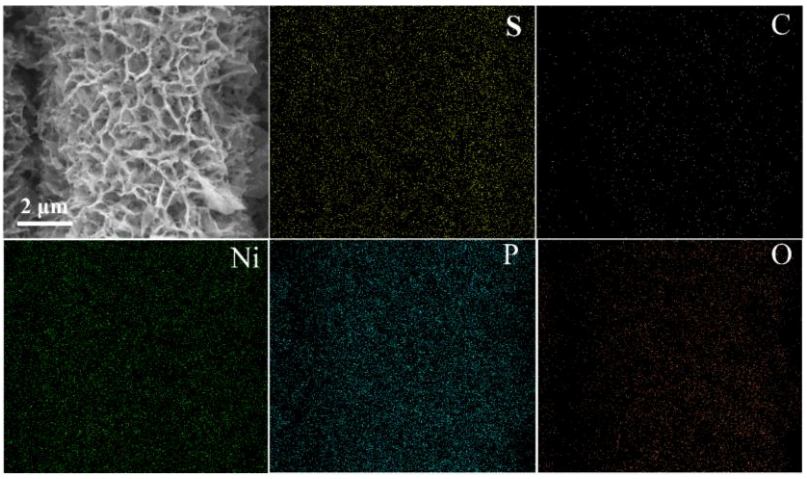

Fig. S9. SEM image and corresponding elemental mappings of S/$Ni(OH)_2$-Ni_2P@CC.

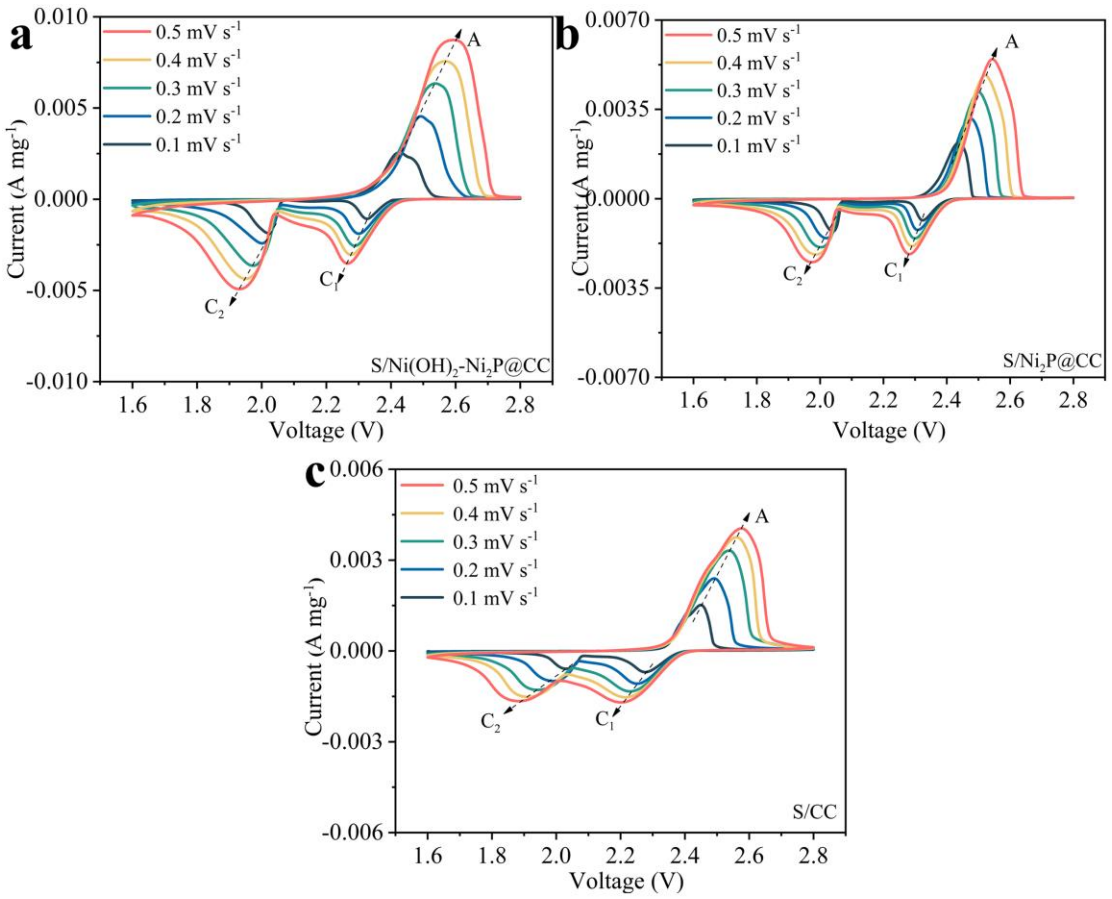

Fig. S10. CV curves of (a) S/Ni(OH)$_2$-Ni$_2$P@CC-based cell, (b) S/Ni$_2$P@CC-based cell and (c) S/CC-based cell at scan rates of 0.1-0.5 mV s^{-1}.

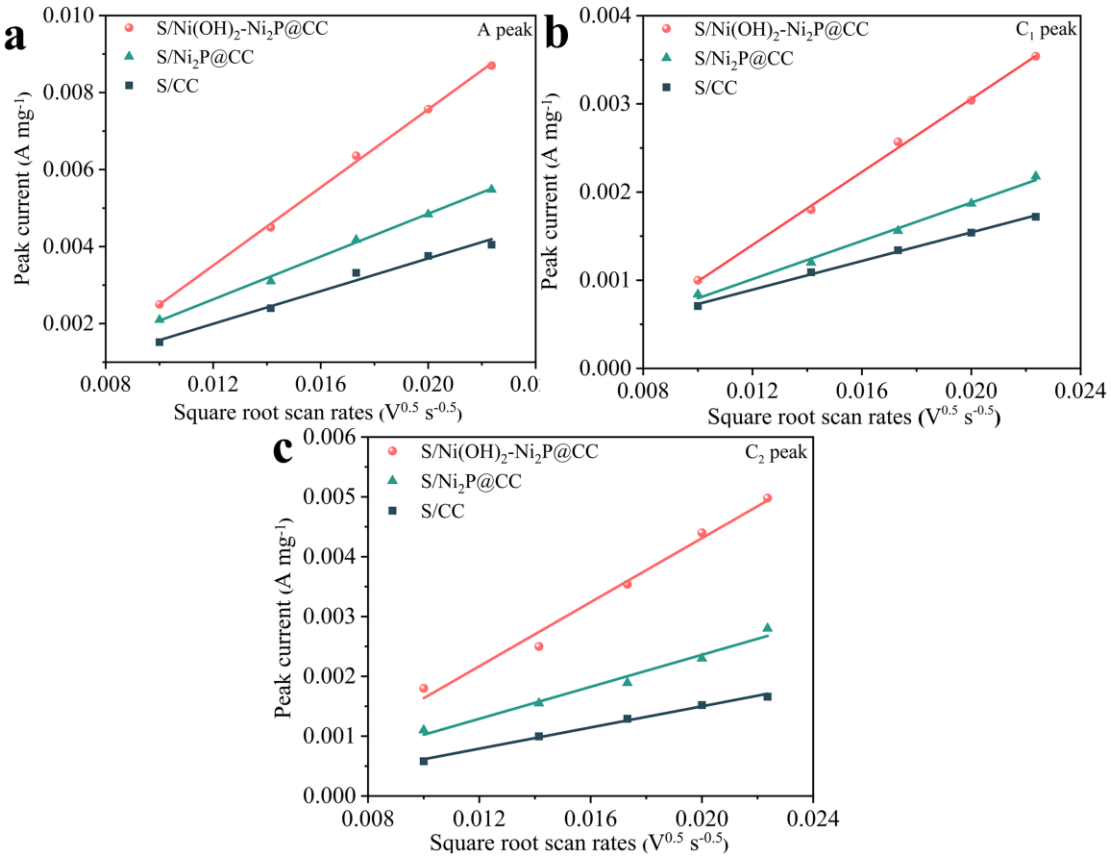

Fig. S11. (a) anodic oxidation process (peak A: $Li_2S/Li_2S_2 \rightarrow S_8$). (b) first cathodic reduction process (peak C_1: $S_8 \rightarrow Li_2S_x$, $4 \leq x \leq 6$). and (c) second cathodic reduction process (peak C_2: $Li_2S_x \rightarrow Li_2S/Li_2S_2$, $4 \leq x \leq 6$) vs the square root of the scan rates.

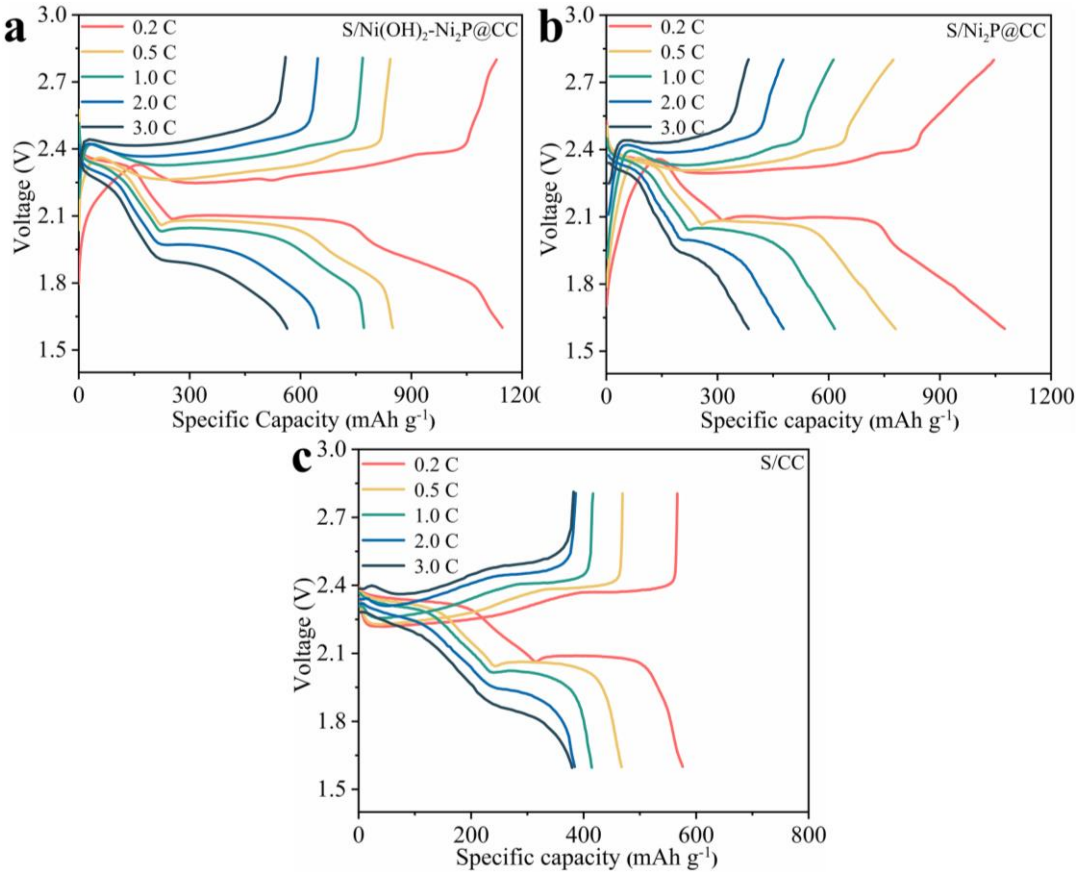

Fig. S12. Charge-discharge profiles of (a) S/$Ni(OH)_2$-Ni_2P@CC-based cell, (b) S/Ni_2P@CC-based cell and (c) S/CC-based cell at different current density.

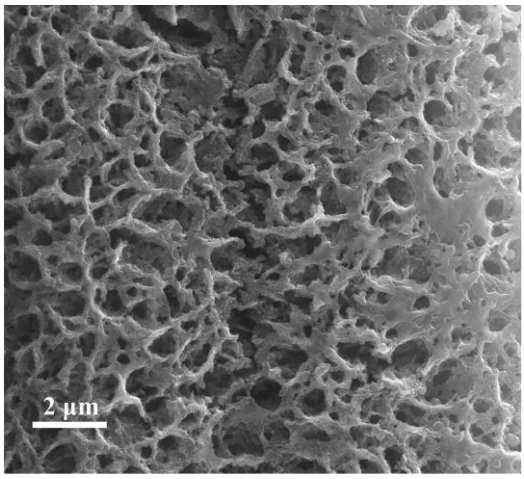

Fig. S13. SEM image of S/Ni(OH)$_2$-Ni$_2$P@CC cathode at fully charged state after 200 cycles at 1 C.

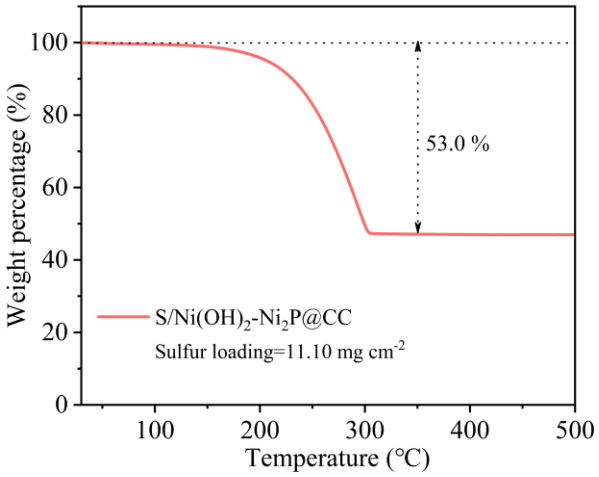

Fig. S14. TGA curve of S/$Ni(OH)_2$-Ni_2P@CC with a high sulfur loading of 11.10 mg cm^{-2}.

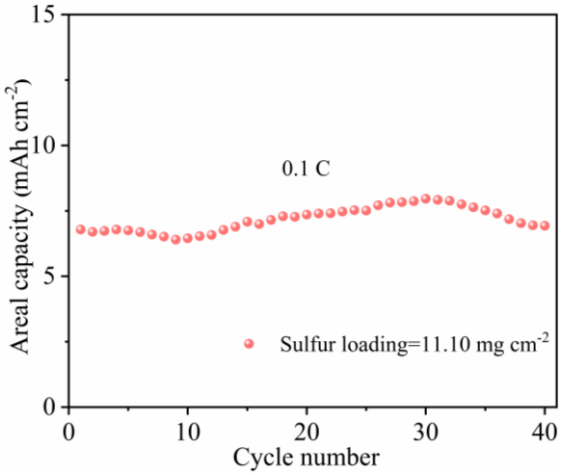

Fig. S15. Cycling performance of S/Ni(OH)$_2$-Ni$_2$P@CC-based cell at 0.1 C even with high sulfur loading (11.10 mg cm^{-2}).

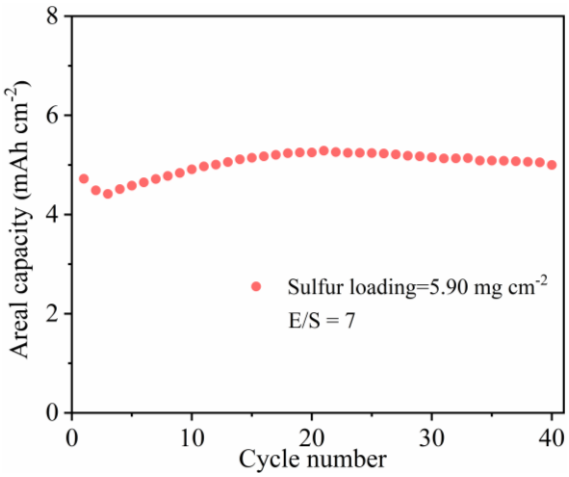

Fig. S16. Cycling performance of S/$Ni(OH)_2$-Ni_2P@CC-based cell with a sulfur loading of 5.90 mg cm^{-2} under the E/S = 7 μL_E $mg^{-1}{}_S$ condition.

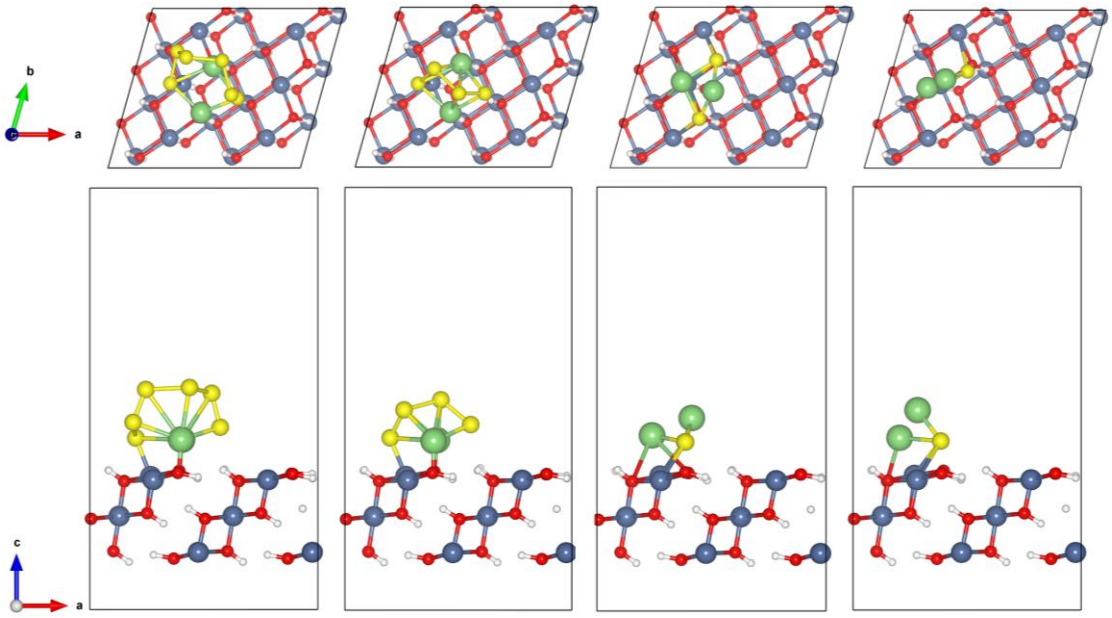

Fig. S17. The optimized adsorption configuration of LiPSs (Li_2S_6, Li_2S_4, Li_2S_2, and Li_2S) adsorbed on the surface of $Ni(OH)_2$.

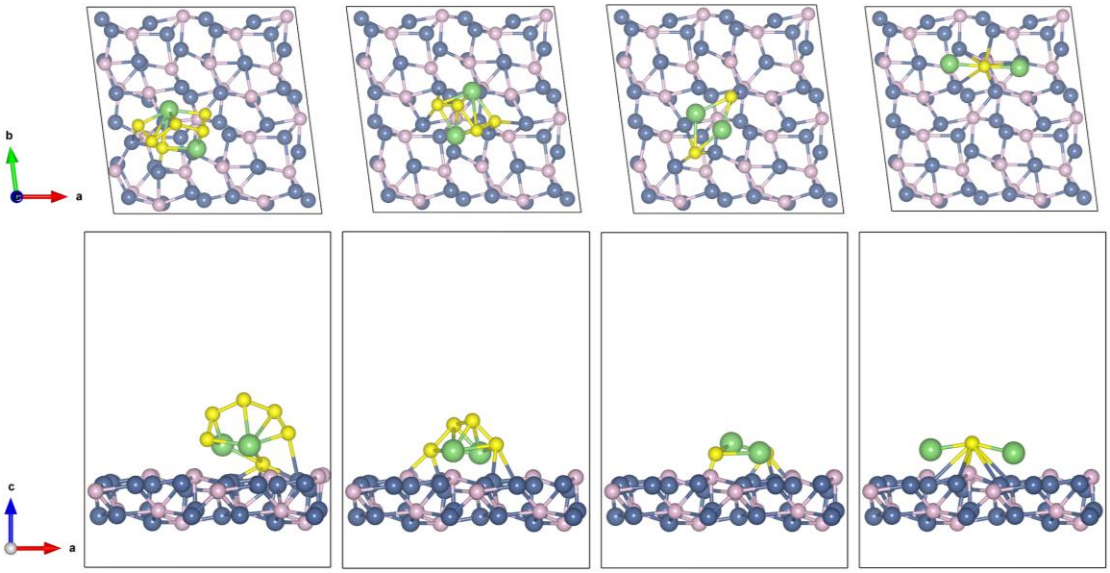

Fig. S18. The optimized adsorption configuration of LiPSs (Li_2S_6, Li_2S_4, Li_2S_2, and Li_2S) adsorbed on the surface of Ni_2P.

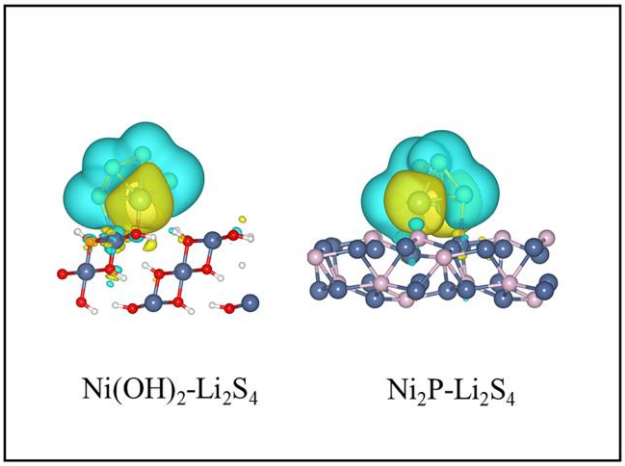

Fig. S19. The charge density difference plots of $Ni(OH)_2$ and Ni_2P after binding with Li_2S_4.

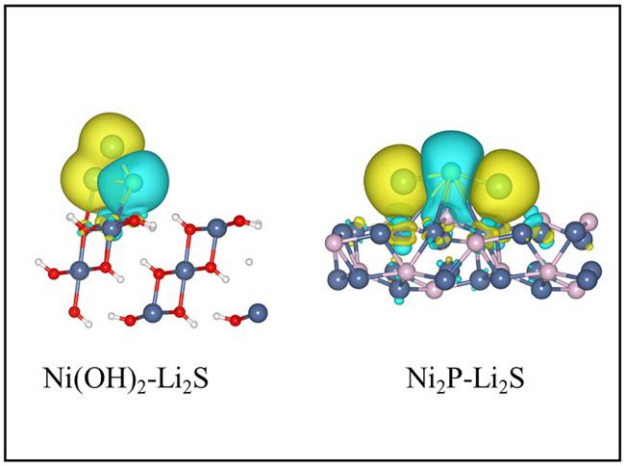

Fig. S20. The charge density difference plots of $Ni(OH)_2$ and Ni_2P after binding with Li_2S.

Table S1. Comparisons of the D_{Li^+} of S/Ni(OH)$_2$-Ni$_2$P@CC, S/Ni$_2$P@CC and S/CC based cells.

Electrode	D_{Li^+}(cm^2 s^{-1})		
	Peak A	Peak C_1	Peak C_2
S/Ni(OH)$_2$-Ni$_2$P@CC	2.70×10^{-7}	4.50×10^{-8}	7.54×10^{-8}
S/Ni$_2$P@CC	8.13×10^{-8}	1.24×10^{-8}	1.88×10^{-8}
S/CC	4.74×10^{-8}	6.97×10^{-9}	8.26×10^{-9}

Table S2. The EIS results of S/Ni(OH)$_2$-Ni$_2$P@CC, S/Ni$_2$P@CC and S/CC based cells before and after cycling.

	Electrode	R_e (Ω)	R_g (Ω)	R_{ct} (Ω)
before cycling	S/Ni(OH)$_2$-Ni$_2$P@CC	2.61	-	22.20
	S/Ni$_2$P@CC	2.39	-	50.00
	S/CC	2.63	-	76.90
after cycling	S/Ni(OH)$_2$-Ni$_2$P@CC	3.65	2.28	4.89
	S/Ni$_2$P@CC	3.26	3.36	10.23
	S/CC	2.67	4.11	15.73

Table S3. The electrochemical performance comparison of the S/$Ni(OH)_2$-Ni_2P@CC-based cell with other articles.

Electrode	Sulfur loading (mg cm^{-2})	E/S ratio (μL mg^{-1})	Rate	Areal capacity (mAh cm^{-2})	Ref
S/$Ni(OH)_2$-Ni_2P@CC	5.9	7.0	0.1 C	5.28	This work
Co/CNT@GF-S	5.1	15.0	0.1 C	4.93	1
CC@CS@HPP/S	5.6	10.0	0.1 C	5.10	2
S-C@MoS_2	4.0	10.0	0.1 C	3.30	3
VSe_2-VG@CC/S	5.5	8.4	0.1 C	4.10	4
Co-NbN/rGO/S	5.6	8.0	0.1 C	3.92	5
BTO-MS-BPC/S	4.5	8.0	0.1C	3.93	6
S-Ni_2Co@rGO	4.0	6.0	0.1 C	4.53	7
3DOM NC@V-ZnO/S	5.8	4.4	0.2 C	4.40	8

Reference

1. Y. Xie, J. Ao, L. Zhang, Y. Shao, H. Zhang, S. Cheng and X. Wang, *Chem. Eng. J.*, 2023, **451**, 139017.

2. Z. Ye, Y. Jiang, L. Li, F. Wu and R. Chen, *Adv. Mater.*, 2020, **32**, 2002168.

3. Q. Wu, Z. Yao, X. Zhou, J. Xu, F. Cao and C. Li, *Acs Nano*, 2020, **14**, 3365-3377.

4. H. Ci, J. Cai, H. Ma, Z. Shi, G. Cui, M. Wang, J. Jin, N. Wei, C. Lu, W. Zhao, J. Sun and Z. Liu, *ACS Nano*, 2020, **14**, 11929-11938.

5. W. Ge, L. Wang, C. Li, C. Wang, D. Wang, Y. Qian and L. Xu, *J. Mater. Chem. A.*, 2020, **8**, 6276-6282.

6. C. Chang, S. Di, G. Gao, B. Zhai, S. Chen, S. Wang, X. Liu and L. Li, *Chem. Eng. J.*, 2022, **435**, 135031.

7. G. Li, W. Qiu, W. Gao, Y. Zhu, X. Zhang, H. Li, Y. Zhang, X. Wang and Z. Chen, *Adv. Funct. Mater.*, 2022, **32**, 2202853.

8. X. Zhao, Y. Guan, X. Du, G. Liu, J. Li and G. Li, *Chem. Eng. J.*, 2022, **431**, 134242.